New Journal of Physics
The open access journal at the forefront of physics

Deutsche Physikalische Gesellschaft DPG IOP Institute of Physics

PAPER • OPEN ACCESS

Propulsion and hydrodynamic particle transport of magnetically twisted colloidal ribbons

To cite this article: Helena Massana-Cid *et al* 2017 *New J. Phys.* **19** 103031

View the article online for updates and enhancements.

Related content

- Driving self-assembly and emergent dynamics in colloidal suspensions by time-dependent magnetic fields
James E Martin and Alexey Snezhko
- Physics of microswimmers—single particle motion and collective behavior: a review
J Elgeti, R G Winkler and G Gompper
- Active colloids
Igor S Aranson

IOP ebooks™

Bringing you innovative digital publishing with leading voices to create your essential collection of books in STEM research.

Start exploring the collection - download the first chapter of every title for free.

This content was downloaded from IP address 161.116.100.31 on 22/06/2018 at 10:37

New Journal of Physics
The open access journal at the forefront of physics

Deutsche Physikalische Gesellschaft DPG
IOP Institute of Physics

Published in partnership with: Deutsche Physikalische Gesellschaft and the Institute of Physics

OPEN ACCESS

RECEIVED
29 May 2017

REVISED
2 August 2017

ACCEPTED FOR PUBLICATION
7 August 2017

PUBLISHED
25 October 2017

Original content from this work may be used under the terms of the Creative Commons Attribution 3.0 licence.

Any further distribution of this work must maintain attribution to the author(s) and the title of the work, journal citation and DOI.

PAPER

Propulsion and hydrodynamic particle transport of magnetically twisted colloidal ribbons

Helena Massana-Cid[1], **Fernando Martinez-Pedrero**[2], **Eloy Navarro-Argemí**[1,3], **Ignacio Pagonabarraga**[1,3] **and Pietro Tierno**[1,3,4]

[1] Departament de Física de la Matèria Condensada, Universitat de Barcelona, E-08028, Barcelona, Spain
[2] Departamento de Química Física I, Universidad Complutense de Madrid, Ciudad Universitaria, E-28040, Madrid, Spain
[3] Universitat de Barcelona Institute of Complex Systems (UBICS), Universitat de Barcelona, E-08028, Barcelona, Spain
[4] Institut de Nanociència i Nanotecnologia, IN^{2}UB, Universitat de Barcelona, E-08028, Barcelona, Spain

E-mail: ptierno@ub.edu

Keywords: low Reynolds number, autonomous actuation, magnetism, fluid-structure interaction, bio-mimetics

Supplementary material for this article is available online

Abstract

We describe a method to trap, transport and release microscopic particles in a viscous fluid using the hydrodynamic flow field generated by a magnetically propelled colloidal ribbon. The ribbon is composed of ferromagnetic microellipsoids that arrange with their long axis parallel to each other, a configuration that is energetically favorable due to their permanent magnetic moments. We use an external precessing magnetic field to torque the anisotropic particles forming the ribbon, and to induce propulsion of the entire structure due to the hydrodynamic coupling with the close substrate. The propulsion speed of the ribbon can be controlled by varying the driving frequency, or the amplitude of the precessing field. The latter parameter is also used to reduce the average inter particle distance and to induce the twisting of the ribbon due to the increase in the attraction between the rotating ellipsoids. Furthermore, non magnetic particles are attracted or repelled with the hydrodynamic flow field generated by the propelling ribbon. The proposed method may be used in channel free microfluidic applications, where the precise trapping and transport of functionalized particles via non invasive magnetic fields is required.

1. Introduction

The trapping and transport of microscopic entities via hydrodynamic flow is an emergent field of research that could lead to novel and exciting developments in lab on a chip devices, such as the controlled release and site specific delivery of chemical or biological cargos. In microfluidic systems, where pressure fields are used to displace nanoliter volumes of reagent in $\sim$100 μm wide channels, the trapping, assembly and positioning of microspheres via hydrodynamic flow has been demonstrated in different works [1–6]. The time reversal nature of fluid flow at low Reynolds (*Re*) number [7] allows for realizing precise single particle operations at the microscale, since inverting the fluid current does not lead to the formation of swirls or turbulence that can randomize the motion of the dispersed particles.

An alternative approach that is gaining much attention is the use of externally driven micropropellers capable to drag and transport microscopic objects using the hydrodynamic flow generated by their movement. This strategy does not require lithographic confinement or externally imposed pressure fields, but a suitable actuation scheme that enables net propulsion at low *Re* number, avoiding reciprocal motion, namely periodic backward and forward body displacements [8]. Recent examples in this direction include the use of magnetically driven nanorods [9], colloidal rotors [10–12], or magnetic particles driven above ferromagnetic structures [13–16]. In contrast to other actuation schemes, for instance the ones based on chemical reactions [17], electric [18], acoustic [19] or optic fields [20], magnetic fields have the advantage of not directly altering the dispersing medium, although they require magnetic parts within the prototypes [21–28].

© 2017 IOP Publishing Ltd and Deutsche Physikalische Gesellschaft

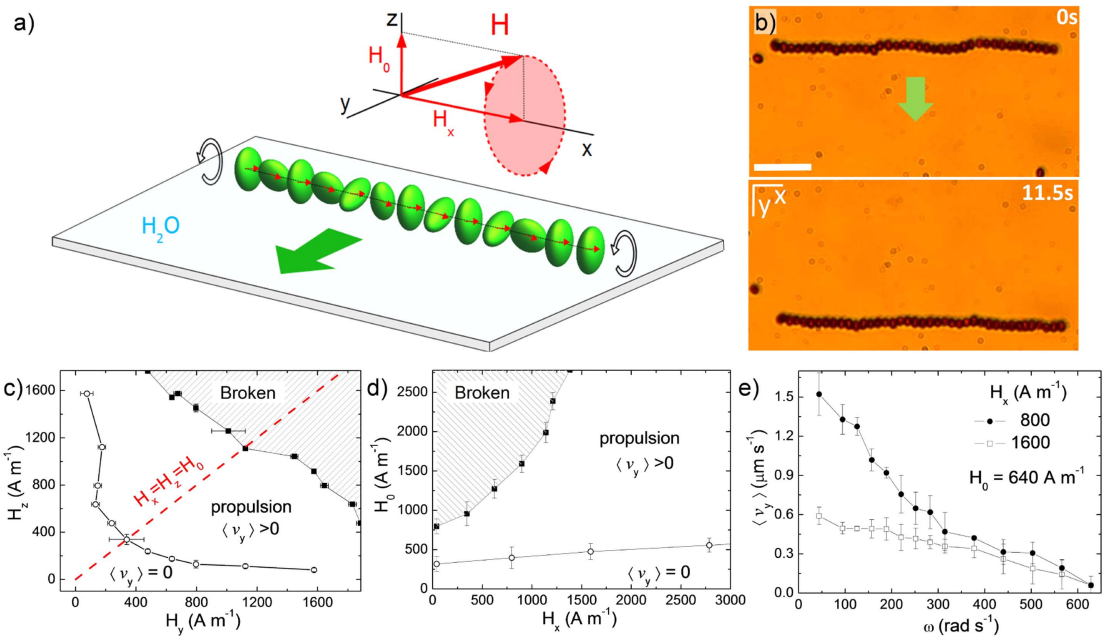

Figure 1. (a) Schematic illustrating a magnetic ribbon composed of 13 ferromagnetic ellipsoids, propelling due to a precessing magnetic field $\boldsymbol{H}$, with amplitudes (H_x, H_0) and angular frequency ω; here $H_0 = H_z = H_y$. (b) Sequence of microscope images showing the transport of one ribbon upon application of a precessing field with $H_0 = 2000$ A m^{-1}, $H_z = 460$ A m^{-1}, and $\omega = 314.2$ rad s^{-1}. The corresponding video can be found in the supporting information which is available online at stacks.iop.org/NJP/19/103031/mmedia. (c) and (d) Diagrams in the (H_y, H_z) plane (c) for $H_0 = 800$ A m^{-1}; and in the (H_x, H_0) plane (d) both for $\omega = 125.7$ rad s^{-1}. The diagrams show the regimes where the ribbons break, propel ($\langle v_y \rangle > 0$) or stop moving ($\langle v_y \rangle = 0$). (e) Average speed $\langle v_y \rangle$ of a ribbon versus driving frequency ω for two amplitudes of the applied field H_x, where $H_0 = 640$ A m^{-1}.

In this article we demonstrate a method to assemble and propel a colloidal ribbon, which is later used to trap and release non magnetic objects in a viscous fluid by using the hydrodynamic flow that it generates. The ribbon is composed by a collection of hematite microellipsoids assembled and propelled upon application of an external precessing magnetic field. The applied field aligns the particles and forces them to rotate in a plane perpendicular to the close surface. The ribbon translates as a whole at a constant speed due to the collective rotations of the composing particles, generating a net flux with a major component perpendicular to its long axis. This hydrodynamic flow is used to manipulate unbound non magnetic particles in a fluid, by attracting or repelling them depending on the sense of rotation of the ellipsoids forming the ribbon. We develop a theoretical model that allows us to compute the generated hydrodynamic flow by using analytical arguments, and to obtain a good agreement with the experimental data.

2. Experimental

The colloidal ribbon is composed of hematite (α-Fe_2O_3) microellipsoids, synthesized following the method developed by Sugimoto and coworkers [29]. The realized particles are monodisperse prolate ellipsoids with a major axis (two minor axes) equal to 1.80 ± 0.11 μm (1.31 ± 0.12 μm resp.). During the synthesis, the particles acquire a permanent moment oriented mainly perpendicular to their long axis, as shown in the schematic in figure 1(a). The non magnetic particles used as a cargo are commercial aqueous suspensions of monodisperse silicon dioxide particles (44054 Sigma-Micro, Sigma-Aldrich), having 4 μm in size. Before the experiments, we first disperse the particles in high deionized water (milliQ, Millipore), stabilize them with sodium dodecyl sulfate (0.11 g of SDS for 80 ml of water) and finally adjust the pH of the solution to 9.5, by adding different aliquots of tetramethylammonium hydroxide. This procedure avoids irreversible sticking between the particles and to the glass surface, induce by attractive Van der Waals interactions. The resulting solution is introduced in a sealed capillary chamber (inner dimensions 0.1–2.00 mm, CMC Scientific), where the particles sediment due to density mismatch. After few minutes, the ellipsoids float at a certain distance above the bottom plate due to balance between gravity and electrostatic repulsive interactions with the surface. We visualize the particle dynamics with an upright optical microscope (Eclipse Ni, Nikon) connected to a CCD camera (Balser Scout scA640-74fc) equipped with a 100× 1.3 NA oil immersion objective.

The precessing field used to propel the magnetic ribbon is generated with a custom made system composed by three coils with their main axis aligned along the three orthogonal directions ($\hat{x}$, $\hat{y}$, $\hat{z}$). The whole

experimental setup is oriented in such a way that the $\hat{x}$ axis coincides with the direction of the Earth magnetic field. In order to generate a rotating magnetic field in the $(\hat{y}, \hat{z})$ plane, i.e. perpendicular to the glass substrate, two pairs of coils are connected to a power amplifier (IMG STA-800, Stage Line) that is commanded by an arbitrary waveform generator (TGA1244, TTi). To apply a constant field along the $\hat{x}$ direction, the third coil is connected to a DC power supply (EL 302RT, TTi).

3. Ribbon assembly and propulsion

In absence of any external field ($\boldsymbol{H} = 0$), the hematite ellipsoids spontaneously assemble into chains or rings due to attractive dipolar interactions arising from their permanent magnetic moments [30]. In a previous work [31], we investigated the orientational dynamics of individual ellipsoids under a static external field and measured an average magnetic moment of $m = 2.3 \times 10^{-16}$ A m^2. Since this moment is perpendicular to the long axis of the ellipsoid, when chaining the particles arrange side by side, forming a ribbon. This configuration is similar to that previously found for ferromagnetic Janus rods, that also showed a magnetization along their short axis [32]. The assembled structure however is rather fragile, and can be easily broken by thermal fluctuations. As a matter of fact, the interaction energy between two isolated ellipsoids at close contact can be estimated as: $U_m = \mu_0 m^2/(4\pi a^3) \sim 0.4 k_B T$, being $\mu_0 = 4\pi \times 10^{-7}$ H m^{-1}, k_B the Boltzmann constant and $T = 293$ K the room temperature. This interaction may increase within the ribbon due to nearest particles, but still it would be of the order of few $k_B T$.

We strengthen and propel the ribbon along a defined direction, in this particular case the $\hat{y}$ axis, by applying an external precessing magnetic field, composed by a static component of amplitude H_x and aligned along the x-axis, and a rotating one polarized in the perpendicular plane $(\hat{y}, \hat{z})$, figure 1(a). The applied field is thus given by: $\boldsymbol{H} = H_x\hat{x} + H_0(\cos(\omega t)\hat{y} - \sin(\omega t)\hat{z})$, where $H_0 = \sqrt{(H_y^2 + H_z^2)/2}$ corresponds to the amplitude of the rotating field and ω its angular frequency. This field has different effects on the chain of ellipsoids. First, the component H_x orients the ribbon along the x axis, minimizing the magnetostatic and the effective demagnetizing energy densities [31]. This effect makes the chain stiffer, as it further aligns the particle moments along the ribbon axis. Second, the rotating component applies a net torque to the ellipsoids, $\boldsymbol{\tau}_m = \mu_0 \boldsymbol{m} \times \boldsymbol{H}$, forcing them to rotate around their short axis. The existence of this torque is due to the fact that, within each ellipsoid, the permanent moments are not exactly perpendicular to the particles' long axis as in an ideal situation, but they have a narrow tilt angle distribution that arises from imperfections during the chemical growth process. This distribution was assessed for isolated particles by measuring the angles between the long axis of the ellipsoids and the direction of a constant applied field, and it is shown in the supporting information[5]. The rotation of the individual ellipsoids within the ribbon is essential for inducing its net displacement. Since the ellipsoids are close to a surface, their rotational motion is rectified in a rolling dynamics, and the ribbon moves as a whole at a constant average speed and along a direction that is dictated by the chirality of the rotating field, figure 1(b).

We first vary the different amplitudes of the precessing field in order to determine the range of experimental values where the propelling ribbons are observed. In the diagram in figure 1(c), we keep constant the static field H_x while varying the ellipticity of rotating field, defined as $\beta = (H_z^2 - H_y^2)/(H_z^2 + H_y^2)$ [33]. The red line cutting in half the diagram denotes the circularly polarized case where $\beta = 0$ ($H_y = H_z = H_0$). The ribbon is propelled for both positive ($H_z > H_y$) and negative ($H_z < H_y$) values of β, while it breaks for large field amplitudes, $H_0 > 1200$ A m^{-1}. The ribbon rupture results from the fact that the magnetic torque is now able to spin the entire structure, and the ribbon behaves as a compact rod that tries to follow the conical precession of the field. However, the magnetic chain inevitably breaks when standing up due to the presence of the solid substrate and the action of gravity. Below $H_0 \sim 400$ A m^{-1}, the magnetic actuation is too weak to induce any propulsive motion. When considering a rotating field circularly polarized ($\beta = 0$), the propelling ribbons are stable for a wide range of values of H_x, as shown in figure 1(d). The tendency to break or to stop propulsion are found for large and small values of H_0 respectively, in agreement with the previous graph. We note that $\langle v_y \rangle = 0$ was defined as the condition accomplished when the average translational motion of the ribbon cannot be distinguished by the one observed in absence of the precessing field, i.e. when the motion of the ellipsoids is due to sole thermal fluctuations.

The average speed of the ribbon $\langle v_y \rangle$ can be easily tuned by varying two control parameters, namely ω and H_x. We start by measuring the dependence of $\langle v_y \rangle$ with ω, and at constant H_x, figure 1(e). For most of the magnetic propellers that are actuated by time dependent fields, the driving frequency is the natural parameter used to control their speed. The frequency allows for changing the particle dynamics from a synchronous regime, where

[5] See supporting information for two videos illustrating the propulsion of one individual ribbon and the controlled hydrodynamic trapping on a silica microsphere.

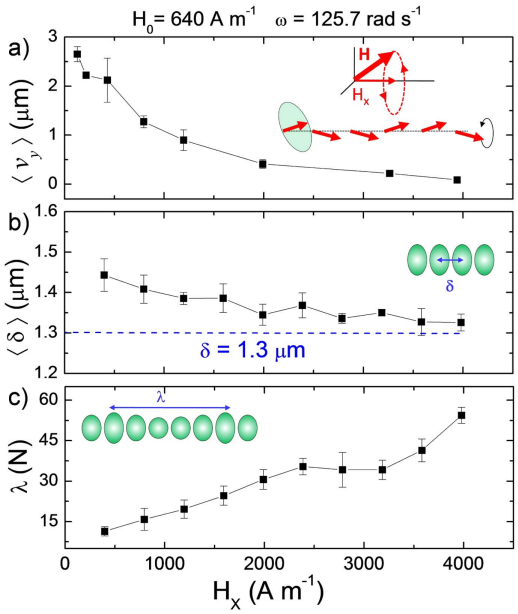

Figure 2. (a)–(c) Average translational speed $\langle v_y \rangle$ (a), inter particle distance $\langle \delta \rangle$ (b) and wavelength λ (c) versus H_x for ribbons composed by hematite ellipsoids. The precessing field has $H_0 = 640$ A m^{-1} and $\omega = 125.7$ rad s^{-1}. The small schematics in the images illustrate the effect of the component H_x on the alignment of the magnetic moments (a), the average distance δ (b) and the wavelength measured in terms of the number of particles N (c).

velocity of the propeller is proportional to the driving frequency, to an asynchronous one, where $\langle v_y \rangle$ decreases as ω increases since the propeller is slower than the field rotations. We find that, for our magnetic ribbons, the rotations of the ellipsoids are in the asynchronous regime for all the explored frequencies, $\omega \in [10,\ 650]$ rad s^{-1}. In this regime of motion the phase angle ϕ between the direction of the magnetic field and the orientation of the permanent moment follows the Adler equation [34] with $\dot{\phi} = \omega - \omega_c \sin(2\phi)$, being ω_c the critical frequency that separates the synchronous from the asynchronous motion. Solving the previous equation for $\omega > \omega_c$ gives the average rotational speed as $\langle \Omega \rangle = \omega(1 - \sqrt{1 - (\omega_c/\omega)^2})$ [35]. Thus, in the asynchronous regime the hematite ellipsoids rotate with an angular frequency $\langle \Omega \rangle$ smaller than the driving frequency ω, showing characteristic 'back and forth' oscillations within the ribbon.

The relative low value of the average speed found, as compared to other magnetic rotors [36–40] results from both, the strongly constrained motion of the particles within the ribbon, and from the small tilt angle of their permanent moments. For $H_x = 800$ A m^{-1}, the average speed $\langle v_y \rangle$ decreases with ω, starting from $\langle v_y \rangle = 1.5\ \mu$m s^{-1} ($\omega = 43.9$ rad s^{-1}) and reducing to zero at $\omega = 628.3$ rad s^{-1}. From the data in figure 1(e) it also emerges that an increase in the amplitude of the in plane field H_x decreases the particle rotational motion and thus the velocity $\langle v_y \rangle$. However, both curves display similar trends beyond $\omega \sim 300$ rad s^{-1} which could be an indication that a different mechanism such as magnetic relaxation [41] becomes dominant at high frequency.

We next characterize the average speed $\langle v_y \rangle$ and the deformation induced by the increase in the amplitude of the static component H_x, while keeping constant ω. The observed trend is similar to that of varying ω, since $\langle v_y \rangle$ decreases as H_x increases, figure 2(a). However, as shown in the small schematic in figure 1(a), the field component H_x is also responsible for the degree of alignment of the particle moments, since it determines the cone angle of the precessional motion described by the ellipsoids. At high values of H_x, the average inter particle distance $\langle \delta \rangle$ reduces linearly towards the the hard sphere limit $\delta = 1.3\ \mu$m, figure 2(b). A direct consequence of this compression is that the colloidal particles experience stronger dipolar attractions that forces them to rotate in a collective manner. Thus, the colloidal chain assumes a twisted conformation, with groups of particles rotating together. The ellipsoidal shape of the particles allows for characterizing this field induced distortion, and the wavelength of the twist can be measured in terms of the average number of particles contained in a complete turn. This number increases almost linearly with H_x, as δ reduces. For very large field values, all the ellipsoids within the ribbon try to rotate together, and the twisting reaches the size of the entire structure, while $\langle v_y \rangle$ goes to zero. The twisted ribbon resembles the helical ribbon formed by paramagnetic colloids subjected to a precessing magnetic field [42]. However, in our case the pitch remains constant along the chain, and no transversal motion of domain walls was observed as in [42].

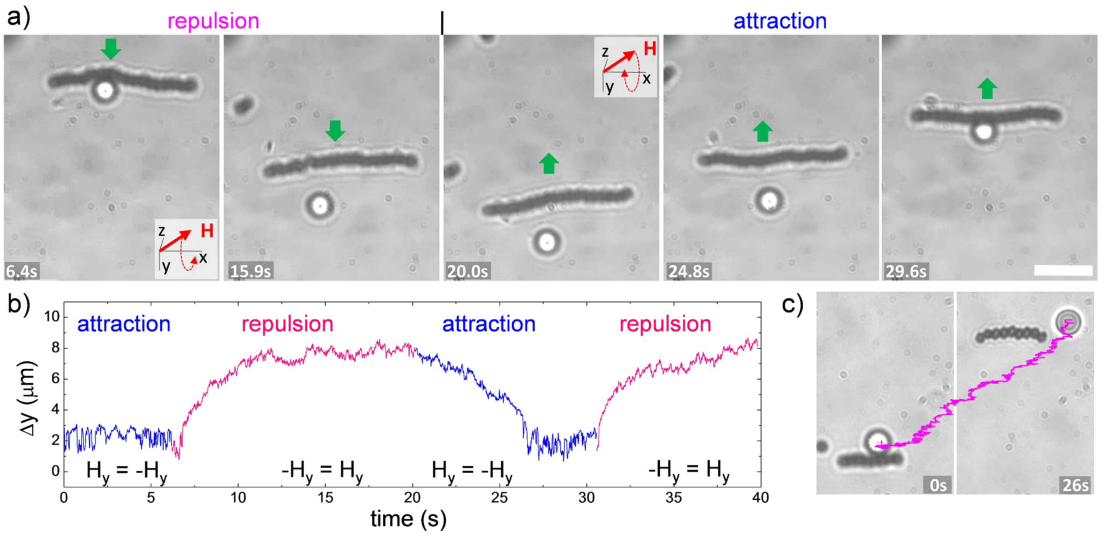

Figure 3. (a) Sequence of microscope images showing how the motion of one silica particle (diameter 4 μm), placed above the glass surface, is controlled by a propelling ribbon subjected to a precessing field of amplitudes $H_0 = 640$ A m^{-1}, $H_z = 80$ A m^{-1} and angular frequency $\omega = 125.7$ rad s^{-1}. (b) Corresponding distance Δy between the center of the ribbon and the center of the silica particle versus time. Blue (magenta) regions indicate hydrodynamic attraction (repulsion) induced by the translation of the ribbon. The reverse of the field H_y, that changes the polarity of the rotating field and consequently the propulsion direction of the ribbon is shown at the bottom of the graph. (c) Images showing two snapshots of one silica particle being repelled by a short ribbon composed of $N = 9$ hematite ellipsoids. The trajectory of the particle is superimposed as a magenta line.

4. Transport of non magnetic colloids

The magnetic ribbons can trap and transport non magnetic particles by using the hydrodynamic flow generated by the rotations of the composing particles. We demonstrate this feature in figure 3(a), where we drive a colloidal ribbon close to a large silica particle of 4 μm diameter. We find that the non magnetic colloid can be either repelled or attracted when located in front or behind the propelling chain, respectively. Even though the ribbon has a finite extension, this length can be much larger than the silica bead diameter, and the latter can be stably trapped and transported when located close to the central part of the ribbon, see the corresponding supplementary video (see footnote 5). By tracking the relative distance Δy between the particle and the central position of the ribbon, figure 3(b), we observe that in both cases, i.e. when located in front or behind the chain, the silica colloid reaches a constant distance from the center of the ribbon. When attracted, the non magnetic particles reaches the back of the chain and remains there as long as the precessing field is applied. Inverting the polarity of one of the two components of the rotating field, here $H_y = -H_y$, reverses the sense of motion of the ribbon. Now the cargo becomes repelled, moving away from the chain till reaching a mean distance of $\Delta y = 8$ μm. The silica cargo can be further localized in a given place by applying a driving frequency higher than $\omega = 600$ rad s^{-1}, so that the chain does not propel but it still generates an attractive flow in its back. An alternative way to trap the non magnetic object without moving it away from the observation area and keeping the frequency constant, would be to periodically switch the sign of H_y. This procedure would allow changing from attraction to repulsion and thus moving the particles back and forth along the same path, confining the colloid along a narrow line. We also find that this hydrodynamic trapping mechanism becomes less stable for shorter ribbons. As shown in figure 3(c), and corresponding VideoS3 (see footnote 5), when transported by a shorter ribbon composed of $N = 9$ particles, the silica colloid eventually escapes from the lateral direction. This indicates that the repulsive hydrodynamic flow is only strictly perpendicular to the ribbon long axis at its center, while it becomes tilted near the edge. This effect can be however minimized by placing the ribbon such that it attracts the non magnetic object at its center.

5. Flow generated by the propelling ribbon

The magnetic ribbon generates a net hydrodynamic flow due to the rotation of the constituent particles. We model this flow by considering the translating chain of ellipsoids as a line of equally spaced particles that rotate close to a solid surface. Direct analytic expressions of the flow produced by this array can be obtained in the Stokes regime, by assuming that each particle has associated an hydrodynamic singularity placed below the solid surface and at the same distance from the solid wall. As described in [43], this singularity is composed by a rotlet,

a stresslet and a source doublet. Thus, the velocity of the flow generated by one colloid rotating at an angular velocity Ω is given by the tensorial equation [43]:

$$\frac{u_i}{a^3} = \frac{\epsilon_{ijk}\Omega_j r_k}{r^3} - \frac{\epsilon_{ijk}\Omega_j R_k}{R^3} + 2h\epsilon_{kjz}\Omega_j\left(\frac{\delta_{ik}}{R^3} - \frac{3R_iR_k}{R^5}\right) + 6\epsilon_{kjz}\frac{\Omega_j R_i R_k R_z}{R^5}. \tag{1}$$

Here r is the position vector from the center of the particle and R the position of its hydrodynamic image, which has an opposite sense of rotation. In this way the tangential component of the generated flow cancels at the interface. Equation (1) can be extended to derive the flow generated by an array of N rotors, aligned along the $\hat{x}$ direction, and rotating with an angular velocity $\tilde{\Omega}_n\hat{y}$, where the index $n = 1 \ldots N$. The rotors are placed at position $\left(0,\ \Delta\left(\frac{N-1}{2} - n\right),\ h_n\right)$, being h_n their elevation from the surface. The velocity field at any point of space $(x,\ y,\ z)$ is given by:

$$u_x = \sum_{n=0}^{N-1} a_n^3\tilde{\Omega}_n\left(\frac{z - h_n}{\left(x^2 + \left(y - \Delta\left(\frac{N-1}{2} - n\right)\right)^2 + (z - h_n)^2\right)^{3/2}}\right.$$

$$\left. + \frac{h_n - z}{\left(x^2 + \left(y - \Delta\left(\frac{N-1}{2} - n\right)\right)^2 + (z + h_n)^2\right)^{3/2}} + \frac{6zx^2}{\left(x^2 + \left(y - \Delta\left(\frac{N-1}{2} - n\right)\right)^2 + (z + h_n)^2\right)^{5/2}}\right), \tag{2}$$

$$u_y = \sum_{n=0}^{N-1} a_n^3\tilde{\Omega}_n\frac{6zx\Delta\left(\frac{N-1}{2} - n\right)}{\left(x^2 + \left(y - \Delta\left(\frac{N-1}{2} - n\right)\right)^2 + (z + h_n)^2\right)^{5/2}}, \tag{3}$$

$$u_z = \sum_{n=0}^{N-1} a_n^3\tilde{\Omega}_n\left(\frac{-x}{\left(x^2 + \left(y - \Delta\left(\frac{N-1}{2} - n\right)\right)^2 + (z - h_n)^2\right)^{3/2}}\right.$$

$$\left. + \frac{x}{\left(x^2 + \left(y - \Delta\left(\frac{N-1}{2} - n\right)\right)^2 + (z + h_n)^2\right)^{3/2}} + \frac{6xz(z + h_n)}{\left(x^2 + \left(y - \Delta\left(\frac{N-1}{2} - n\right)\right)^2 + (z + h_n)^2\right)^{5/2}}\right). \tag{4}$$

It should be noted that our theoretical model considers only the hydrodynamic contribution, neglecting any further interaction between the particles. The magnetic interactions are important to assemble the chain of particles and to generate the net torque, but do not have any direct influence on the produced hydrodynamic flow. As a matter of fact, such interactions have been already addressed in a different context [30, 31], and here we assume that the ellipsoids rotates at an average angular velocity $\langle\tilde{\Omega}\rangle$. Using equation (1) it also possible to determine the average speed for a chain of spherical rotors in a similar way as done in [44], where paramagnetic colloids were magnetically assembled in chains that translated parallel to the surface and along their main axis. However, in our case this calculation may give rise to theoretical values different than the experimental ones due the non spherical shape of our ellipsoids and the asynchronous rotation resulting from the strong dipolar attraction between the particles.

We test our model by first calculating the flow profile generated by a chain of rotors that moves towards the $\hat{y}$ direction, figure 4(a). As expected from the experimental evidence, the flow profile is attractive behind the propelling chain of particles (blue arrows), and repulsive in front of it (magenta arrows). Moreover, it radially converges toward the center of the chain, sign that tracer particles placed close to the border of the chain migrate toward the chain center when attracted, or are expelled from it when are repelled, as observed in figure 3(c).

A quantitative comparison with the experimental data is shown in figure 4(b), where we measure the average speed of the non magnetic tracer particles as a function of the distance from the center of a ribbon, which is propelled at different speeds obtained by varying the amplitude of H_x. We then perform multiple fits to the experimental data (scattered data in figure 4(b)) by using equation (2) of the model. In all cases, the experimental parameters that we kept fixed are the radius of the rotating particles, $r = 0.65\ \mu$m, their elevation $h = 0.75\ \mu$m, mean distance $\delta = 1.3\ \mu$m and the elevation of the silica particle $H = 2.1\ \mu$m. We then leave as the only adjustable parameter the average angular rotation of the ellipsoids $\langle\tilde{\Omega}\rangle$, that is induced by the precessing field.

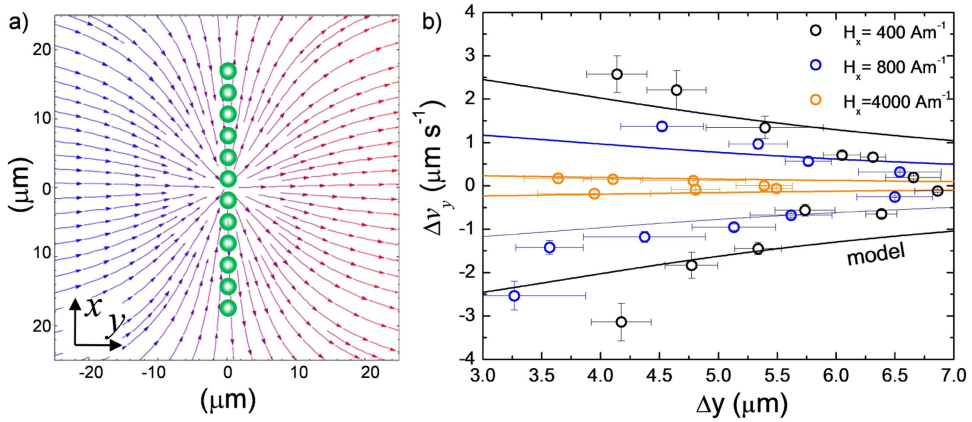

Figure 4. (a) Streamplot of the flow velocity u_y generated by a chain of $N = 12$ propellers translating from left to right. The velocity field was calculated at the same elevation of the chain, see model in the text. The flow is attractive behind the chain (blue arrows), and repulsive in front of it (magenta arrows). (b) Flow velocity u_y versus distance Δy when the particle is repelled ($u_y > 0$) or attracted ($u_y < 0$) by a propelling ribbon driven by a precessing field with $H_0 = 640$ A m^{-1} and angular frequency $\omega = 125.7$ rad s^{-1}. Scattered points are experimental data taken at different amplitudes of the in plane field H_x. Continuous lines are multiple fits to equation (2) of the model.

The values of $\langle\tilde{\Omega}\rangle$ obtained from the fits are always smaller than the field frequency ω, confirming the fact that the particles rotates asynchronously with the driving field. For short distances or small speed of the chain (high values of H_x), there is a good agreement with the experimental data, even if the developed model present different approximations. At large separations between the ribbon and the silica particle, some deviations from the theoretical trend become visible. At such distances, thermal fluctuations may be strong enough to perturb the particle trajectory, or the effect of the finite size of the chain may become significant.

6. Conclusions

In this article we have demonstrated a method to trap and transport non magnetic objects in a viscous fluid by using a magnetically assembled and twisted chain of rotating ferromagnetic ellipsoids. The chain propulsion is induced by an external precessing field, that allows for tuning both the chain mean speed and the twisted conformation. We describe the generated hydrodynamic flow as the cooperative flow resulting from a one dimensional ensemble of microscopic rotors. Even though our theoretical approach uses far field approximations, it properly captures the physics behind the hydrodynamic trapping process. Further extension of this study may include the effect of the magnetic interactions between the particles and how these interactions lead to the twisted state. On the application side, our magnetic twisted ribbon may be potentially used in lab on a chip devices where precise transport of non magnetic objects is required for the delivery of drugs or chemicals attached to functionalized particles.

Acknowledgments

HMC and PT acknowledge support from the ERC starting Grant 'DynaMO' (No. 335040). FMP acknowledges support from the Ramón y Cajal program (RYC-2015-18495). PT acknowledges support from MINECO (FIS2016-78507-C2-2-P) and DURSI (2014SGR878). EN and IP acknowledge support from MINECO (Spain), Project FIS2016-78507-C2-2-P, DURSI Project 2014SGR-922, and Generalitat de Catalunya under Program 'ICREA Acadèmia'.

References

[1] Lutz B R, Chen J and Schwartz D T 2006 Hydrodynamic tweezers: 1. Noncontact trapping of single cells using steady streaming microeddies *Anal. Chem.* **15** 5429–35
[2] Lin C M, Lai Y S, Liu H P, Chen C Y and Wo A W 2008 Trapping of bioparticles via microvortices in a microfluidic device for bioassay applications *Anal. Chem.* **23** 8937–45
[3] Schneider T M, Mandre S and Brenner M P 2011 Algorithm for a microfluidic assembly line *Phys. Rev. Lett.* **106** 094503
[4] Karimi A, Yazdi S and Ardekani A M 2013 Hydrodynamic mechanisms of cell and particle trapping in microfluidics *Biomicrofluidics* **7** 021501
[5] Tanyeri M and Schroede C M 2013 Manipulation and confinement of single particles using fluid flow *Nano Lett.* **12** 2357–64

[6] Zhou Y, Basu S, Wohlfahrt K J, Leec S F, Klenerman D, Laue E D and Seshia A A 2016 A microfluidic platform for trapping, releasing and super-resolution imaging of single cells *Sensors Actuators* B **232** 680–91
[7] Happel J and Brenner H 1973 *Low Reynolds Number Hydrodynamics* (Leiden: Noordhoff)
[8] Purcell E M 1977 Life at low reynolds number *Am. J. Phys.* **45** 3
[9] Petit T, Zhang L, Peyer K E, Kratochvil B E and Nelson B J 2012 Selective trapping and manipulation of microscale objects using mobile microvortices *Nano Lett.* **12** 156–60
[10] Sing C E, Schmid L, Schneider M F, Franke T and Alexander-Katz A 2010 Controlled surface-induced flows from the motion of self-assembled colloidal walkers *Proc. Natl Acad. Sci. USA* **107** 535–40
[11] Martinez-Pedrero F and Tierno P 2015 Magnetic propulsion of self-assembled colloidal carpets: efficient cargo transport via a conveyor-belt effect *Phys. Rev. Appl.* **3** 051003
[12] Driscoll M, Delmotte B, Youssef M, Sacanna S, Donev A and Chaikin P 2017 Unstable fronts and motile structures formed by microrollers *Nat. Phys.* **13** 375–9
[13] Yellen B B, Hovorka O and Friedman G 2005 Arranging matter by magnetic nanoparticle assemblers *Proc. Natl Acad. Sci. USA* **102** 8860–4
[14] Tierno P, Reddy S V, Yuan J, Johansen T H and Fischer T M 2007 Transport of loaded and unloaded microcarriers in a colloidal magnetic shift register *J. Phys. Chem.* B **111** 13479–82
[15] Martinez-Pedrero F, Straube A V, Johansen T H and Tierno P 2015 Functional colloidal micro-sieves assembled and guided above a channel-free magnetic striped film *Lab Chip* **15** 1765–71
[16] Yang T, Tasci T O, Neeves K B, Ning W N and Marr D W M 2017 Magnetic microlassos for reversible cargo capture, transport and release film *Langmuir* **33** 5932–7
[17] Howse J R, Jones R A L, Ryan A J, Gough T, Vafabakhsh R and Golestanian R 2007 Self-motile colloidal particles: from directed propulsion to random walk film *Phys. Rev. Lett.* **99** 048102
[18] Bricard A, Caussin J-B, Desreumaux N, Dauchot O and Bartolo D 2013 Emergence of macroscopic directed motion in populations of motile colloids *Nature* **503** 95
[19] Wang W, Castro L A, Hoyos M and Mallouk T E 2012 Autonomous motion of metallic microrods propelled by ultrasound *ACS Nano* **6** 6122–32
[20] Volpe G, Buttinoni I, Vogt D, Kümmerer H-J and Bechinger C 2011 Microswimmers in patterned environments *Soft Matter* **7** 8810–5
[21] Dreyfus R, Baudry J, Roper M L, Fermigier M, Stone H A and Bibette J 2005 Microscopic artificial swimmers *Nature* **437** 862
[22] Snezhko A, Belkin M, Aranson I S and Kwok W K 2009 Self-assembled magnetic surface swimmers *Phys. Rev. Lett.* **102** 118103
[23] Zhang L, Abbott J J, Dong L, Peyer K E, Kratochvil B E, Zhang H, Bergeles C and Nelson B J 2009 Characterizing the swimming properties of artificial bacterial flagella *Nano Lett.* **9** 3663–7
[24] Ghosh A and Fischer P 2009 Controlled propulsion of artificial magnetic nanostructured propellers *Nano Lett.* **9** 2243
[25] Pak O S, Gao W, Wang J and Lauga E 2011 High-speed propulsion of flexible nanowire motors: theory and experiments *Soft Matter* **7** 8169–81
[26] Lumay G, Obara N, Weyer F and Vandewalle N 2013 Self-assembled magnetocapillary swimmers *Soft Matter* **9** 2420
[27] Dobnikar J, Snezhko A and Yethiraj A 2013 Emergent colloidal dynamics in electromagnetic fields *Soft Matter* **9** 3693–704
[28] Tierno P 2014 Recent advances in anisotropic magnetic colloids: realization, assembly and applications *Phys. Chem. Chem. Phys.* **16** 23515
[29] Sugimoto T, Khan M M and Muramatsu A 1993 Preparation of monodisperse peanut-type alpha-Fe_2O_3 particles from condensed ferric hydroxide gel *Colloids Surf.* A **70** 167
[30] Martinez-Pedrero F, Cebers A and Tierno P 2016 Dipolar rings of microscopic ellipsoids: magnetic manipulation and cell entrapment *Phys. Rev. Appl.* **6** 034002
[31] Martinez-Pedrero F, Cebers A and Tierno P 2016 Orientational dynamics of colloidal ribbons self assembled from microscopic magnetic ellipsoids *Soft Matter* **12** 3688–95
[32] Yan J, Chaudhary K, Chul Bae S, Lewis J A and Granick S 2013 Colloidal ribbons and rings from Janus magnetic rods *Nat. Commun.* **4** 15162
[33] Lacis S, Bacri J C, Cebers A and Perzynski R 1997 Frequency locking and devil's staircase for a two-dimensional ferrofluid droplet in an elliptically polarized rotating magnetic field *Phys. Rev.* E **55** 2640
[34] Adler R 1946 A study of locking phenomena in oscillators *Proc. IRE* **34** 351
[35] Tierno P, Claret J, Sagués F and Cebers A 2009 Overdamped dynamics of paramagnetic ellipsoids in a precessing magnetic field *Phys. Rev.* E **79** 021501
[36] Morimoto H, Ukai T, Nagaoka Y, Grobert N and Maekawa T 2008 Tumbling motion of magnetic particles on a magnetic substrate induced by a rotational magnetic field *Phys. Rev.* E **78** 021403
[37] Janssen X J, Schellekens A J, van Ommering K, van Ijzendoorn L J and Prins M W 2009 Controlled torque on superparamagnetic beads for functional biosensors *Biosens. Bioelectron.* **24** 1937
[38] Tierno P, Güell O, Sagués F, Golestanian R and Pagonabarraga I 2010 Controlled propulsion in viscous fluids of magnetically actuated colloidal doublets *Phys. Rev.* E **81** 011402
[39] Tottori S, Zhang L, Qiu F, Krawczyk K K, Franco-Obregón A and Nelson B J 2012 Magnetic helical micromachines: fabrication, controlled swimming, and cargo transport *Adv. Mater.* **24** 811
[40] Tasci T O, Herson P S, Neeves K B and Marr D W M 2016 Surface-enabled propulsion and control of colloidal microwheels *Nat. Commun.* **7** 10225
[41] Cebers A and Kalis H 2011 Dynamics of superparamagnetic filaments with finite magnetic relaxation time *Eur. Phys. J.* E **34** 30
[42] Casic N, Alvarez-Nodarse R, Mertens F G, Jibuti L, Zimmermann W and Fischer T M 2013 Propulsion efficiency of a dynamic self-assembled helical ribbon *Phys. Rev. Lett.* **110** 168302
[43] Blake J R and Chwang A T 1974 Fundamental singularities of viscous flow *J. Eng. Math.* **8** 23–9
[44] Martinez-Pedrero F, Ortiz-Ambriz A, Pagonabarraga I and Tierno P 2015 Colloidal microworms propelling via a cooperative hydrodynamic conveyor belt *Phys. Rev. Lett.* **115** 138301